

Bulk phase behaviour vs interface adsorption: Effects of anions and isotopes on β -lactoglobulin (BLG) interactions

Madeleine R. Fries

Institute for Applied Physics, University of Tübingen, 72076 Tübingen, Germany, email: madeleine.fries@uni-tuebingen.de

Maximilian W. A. Skoda

ISIS Facility, STFC, Rutherford Appleton Laboratory, Didcot, OX11 0QX, United Kingdom, email: maximilian.skoda@stfc.ac.uk

Nina F. Conzelmann

Institute for Applied Physics, University of Tübingen, 72076 Tübingen, Germany, email: nina.conzelmann@student.uni-tuebingen.de

Robert M. J. Jacobs

Department for Chemistry, University of Oxford, Oxford, OX1 3TA, United Kingdom, email: robert.jacobs@chem.ox.ac.uk

Ralph Maier

Institute for Applied Physics, University of Tübingen, 72076 Tübingen, Germany, email: ralph.maier@uni-tuebingen.de

Niels Scheffczyk

Institute for Applied Physics, University of Tübingen, 72076 Tübingen, Germany, email: niels.scheffczyk@student.uni-tuebingen.de

Fajun Zhang

Institute for Applied Physics, University of Tübingen, 72076 Tübingen, Germany, email: fajun.zhang@uni-tuebingen.de

Frank Schreiber*

Institute for Applied Physics, University of Tübingen, 72076 Tübingen, Germany, email: frank.schreiber@uni-tuebingen.de

*Corresponding author, email: frank.schreiber@uni-tuebingen.de, telephone: 0049-7071-29-76058, fax: 0049-7071-29-5110

Abstract

Hypothesis

Protein adsorption is highly relevant in numerous applications ranging from food processing to medical implants. In this context, it is important to gain a deeper understanding of protein-protein and protein-surface interactions. Thus, the focus of this investigation is on the interplay of bulk properties and surface properties on protein adsorption. It was hypothesised that the type of solvent and ions in solution should **significantly** influence the protein's bulk and interface behaviour, **which has been observed in literature and previous work for other net negatively charged, globular proteins such as bovine serum albumin (BSA).**

Experiments

The phase behaviour of β -lactoglobulin (**BLG**) with lanthanum chloride (LaCl_3) and iodide (LaI_3) in **normal water ($\text{H}_2\text{O}(\text{l})$) and heavy water ($\text{D}_2\text{O}(\text{l})$)** was established via optical microscopy and ultraviolet-visible spectroscopy. The formation of an adsorption layer and its properties such as thickness, density, structure, and hydration was investigated via neutron reflectivity, quartz-crystal microbalance with dissipation, and infra-red measurements.

Findings

β -lactoglobulin does not show significant anion-induced or isotope-induced effects - neither in bulk nor at the solid-liquid interface, which deviates strongly from the behaviour of bovine serum albumin. We also provide a comprehensive discussion and comparison of protein-specific bulk and interface behaviour between bovine serum albumin and β -lactoglobulin dependent on anion, cation, solvent, and substrate properties. These findings pave the way for understanding the transition from adsorption to crystallisation.

Keywords: anion, isotope, bulk, adsorption, wetting, QCM-D, NR ¹

¹ATR-FTIR - attenuated total reflectance Fourier-transform infra-red spectroscopy, BLG - β -lactoglobulin, BSA - bovine serum albumin, c^* - boundary between regime I and II, c^{**} - boundary between regime II and III, **Ca^{2+} - calcium(2+) ion**, CI - confidence interval, **Cl^- - chloride**, c_p - protein concentration, c_s - salt concentration, d - adsorbed protein layer

1. Introduction

The human body is composed of roughly 16 % of proteins [1] and has to ingest ideally 180 g per day of dietary proteins to allow proper body function [2, 3]. In Central European countries, these dietary proteins originate to 28 % from meat and meat products, 28 % from milk and dairy products, 3 % from fish, 3 % from eggs, and the rest is of plant origin [4, 5].

The major protein component of bovine whey is β -lactoglobulin (BLG) [6]. The physiological concentration of BLG in cow milk varies between 4 to 20 mg/ml [7]. The main function of BLG is not yet fully established, but it was found to bind and transport small hydrophobic ligands e.g. vitamin D, cholesterol, retinol, and fatty acids [8, 6, 9, 10, 7]. Consequently, it contributes to the milk fatty acid metabolism [7], enzyme regulation, and neonatal acquisition of passive immunity [6]. Its antioxidant properties are a health benefit [11].

On the one hand, BLG does not occur in human milk [12], and it is not surprisingly the most common source for food allergies and (milk) intolerances in humans [13]. On the other hand, it can be used as a natural carrier for e.g. nutraceuticals due to its naturally abundance, biodegradability, and biocompatibility [14]. It allows the enrichment of food with nutrients through protein encapsulation, protein-based emulsions or cross-linked hydrogels [14, 15, 16].

Due to its resistance to acid proteases [17] and gastric digestion *in vivo* [18], BLG stays intact after passing the stomach. This property is not only utilised for incorporation and delivery of nutraceuticals [15], but also for drug

thickness, D - dissipation, $D_2O(l)$ - heavy water, d_{NR} - adsorbed protein layer thickness determined by neutron reflectivity, F - frequency, $H_2O(l)$ - normal water, Ho^{3+} - holmium(3+) ion, Hydr. - hydration of adsorbed layer, I^- - iodide, λ - wavelength, La^{3+} - lanthanum(3+) ion, $LaCl_3$ - lanthanum chloride, LaI_3 - lanthanum iodide, LCST - lower critical solution temperature, LLPS - liquid-liquid phase separation M_W - molecular weight, NR - neutron reflectivity, QCM-D - quartz crystal microbalance with dissipation, Q_z - momentum transfer, RC - re-entrant condensation, R_H - hydrodynamic radius, SiO_2 - silicon dioxide, SLD - scattering length density, σ - layer roughness, θ - incident angle, TOC - total organic carbon, UCST - upper critical solution temperature, UV-vis - ultraviolet-visible, Y^{3+} - yttrium(3+) ion, YCl_3 - yttrium chloride

delivery [19, 14]. Protein-based drug delivery systems enable the transport of otherwise poorly water soluble drugs [20] such as Fenofibrate, Theophylline or
 25 Sulfamethoxazole [21, 16]. Importantly in this context, BLG can crystallise under certain conditions [22]. This facilitates new possibilities for drug purification and stabilisation through the usage of proteins [23]. One approach to control protein crystallisation, e.g. of BLG, is through the addition of multivalent salts [24, 25, 26, 27].

30 Salt is a natural component in food including milk. In food processing, salt is an important ingredient for preservation, stabilisation, and flavour enhancement [28, 29]. BLG is known to naturally bind calcium(2+) ion (Ca^{2+}) [30], which can induce a variety of phase behaviours e.g. salt-induced gelation of BLG based on hydrophobic interactions [30], which finds application in cosmet-
 35 ics [16]. Other multivalent salts, such as yttrium chloride, neodymium chloride, cadmium chloride and zinc chloride, can generate even stronger interactions than Ca^{2+} and were found to induce a rich phase behaviour for BLG featuring re-entrant condensation (RC), liquid-liquid phase separation (LLPS) and protein crystallisation [31, 24, 25, 26, 27, 32]. This illustrates the complexity
 40 and variety of interactions guiding the BLG bulk phase behaviour of competing (electrostatic and hydrophobic) interactions.

Yet, not only the bulk interactions (protein-protein) have to be considered, but also possible interactions with interfaces (protein-interface). The interactions of proteins, such as BLG, with the steel or glass containers and other
 45 components must be understood to allow sterile and contamination-free food processing. The cleaning and processing of these products are based on forced desorption of proteins and anti-fouling surfaces [33, 34]. Certain interface properties can be favoured, e.g charged membranes in filtration systems have been shown to allow better separation of proteins [35]. In this context, the interplay
 50 of bulk and adsorption properties is important to understand and to control.

This study, thus, focuses on BLG and the influence of different anions (LaCl_3 vs LaI_3) and solvents ($\text{H}_2\text{O}(\text{l})$, $\text{D}_2\text{O}(\text{l})$) on its bulk phase behaviour via ultraviolet-visible (UV-vis) spectroscopy, pH, and optical microscopy measure-

ments. In order to test the fine-tuning of interactions [36], we use chloride (Cl^-)
55 and iodide (I^-), which are both naturally occurring in the human body [37, 38]
and critical for numerous body functions [38, 39] in $\text{H}_2\text{O}(\text{l})$ and $\text{D}_2\text{O}(\text{l})$. These
solvents are highly relevant for neutron scattering and vibrational spectroscopy
[40, 41, 42]. New phase diagrams of BLG are established in the presence of
lanthanum(3+) ion (La^{3+}) as the multivalent cation. La^{3+} has a similar size
60 to Ca^{2+} [43], but induces stronger interactions due to its higher charge [44].
Thus, La^{3+} offers a broader range of applications by acting as a model cation
to compare to calcium processes [45] or as a calcium antagonist [46] in form of
e.g. a neurotoxin [47].

In parallel with the bulk behaviour, its adsorption behaviour on a solid, net
65 negatively charged, hydrophilic surface (SiO_2 , mimicking glass) is investigated
with neutron reflectivity (NR), quartz-crystal microbalance with dissipation
(QCM-D), and attenuated total reflectance Fourier-transform infra-red spec-
troscopy (ATR-FTIR), which provides insight into the adsorbed layer thickness
(d), hydration (Hydr.), roughness (σ), and secondary structure. The adsorption
70 process can be viewed as the primary stage of protein crystallisation, namely
nucleation, at interfaces. This is part of an effort to gain a deeper understanding
of protein-protein and protein-surface interactions in the presence of multiva-
lent ions. In the following, a comparison between bovine serum albumin (BSA)
(data from Ref. 48) and BLG is given, illustrating fundamental similarities and
75 differences between the two proteins and how those affect their behaviours in
bulk and at solid interfaces.

2. Materials and methods

2.1. Materials

The materials used were purchased from Sigma Aldrich (now Merck), namely
80 BLG with a purity of $\geq 90\%$ (product No. L3908), LaCl_3 with a purity of
99.99 % (product No. 449830), LaI_3 with a purity of 99.9 % (product No.
413674) and $\text{D}_2\text{O}(\text{l})$ with a purity of 99.9 % (product no. 151882). For the bulk

and adsorption measurements, we prepared salt stock solutions with a concentration of 100 mM in degassed Milli-Q water or D₂O(l), as well as protein stock solutions. The Milli-Q water has a total organic carbon (TOC) value of 1.7 ppb and a resistivity of 18.2 MΩ·cm at 25°C. Most proteins containing aromatic amino acids show an absorbance maximum at 280 nm. Thus, the concentration of the protein stock solution was determined by UV-vis absorbance spectrometer measurements (Cary 50 UV-vis spectrometer, Varian Technologies, USA) scanning from 200 to 400 nm and calculating the concentration from the absorbance with the Beer-Lambert law. The extinction coefficient of BLG at 280 nm is 0.96 ml/(mg·cm) (Tab. 3).

2.2. Bulk phase behaviour

The phase diagrams were determined at protein concentrations c_p of 5, 20, 50, and 80 mg/ml with the respective salts and in the respective solvents. The salt concentration c_s was varied from 0 to 60 mM. The bulk samples were prepared by mixing the proteins with solvent and afterwards adding the desired amount of salt of the salt stock solution of 100 mM. The phase diagrams shown in Fig. 1 were determined by UV-vis transmittance measurements at low c_s (Fig. S2) [49] and visual inspection through the production of a dilution series shown exemplarily in Fig. S1. The first phase boundary at the salt concentration c^* is defined by the onset of turbidity correlated with a drop in transmittance. The second phase boundary c^{**} is determined by calculating the averaged value of the last turbid and the first completely re-cleared solution, for example, shown in the transmittance progression in Fig. S2 and images of the samples in Fig. S1. The error bars depict in the phase diagrams illustrate the systematic and statistical variations of the phase boundaries resulting from protein stalk variations and preparation imprecision. Optical microscopy was used to follow the two-step LLPS formation (Fig. 2).

2.3. Adsorption measurements

All adsorption measurements were performed *in situ* and the adsorption time was set to 1 h, which was sufficiently close to equilibrium conditions, besides

regime II, which shows significantly enhanced adsorption and continuous growth.

All adsorption measurements were performed at c_p (BLG) of 5 mg/ml and at c_s
115 of 0, 0.1, 0.8, and 5 mM in H₂O(l) or D₂O(l).

2.3.1. QCM-D

The classical QCM substrate consists of a thickness-shear mode (AT-cut) quartz crystal between two metal (gold) electrodes [50]. By applying a voltage, mechanical deformations are induced, which lead to the oscillation of the crystal.
120 The resonance frequency (F) of the crystal depends on the total oscillating mass including coupled water. This means by the addition of mass e.g. through adsorption, a change in F (ΔF) can be detected. The QCM-D works in a ring-down scheme meaning the external potential is turned down intermittently and the oscillations can decay freely leading to a measurable voltage through the
125 decaying mechanical oscillations [51] and thus to the two measured parameters: ΔF and the dissipation (decay of voltage) ΔD . Depending on the properties of the adsorbed material, a strong damping of the oscillations can be induced leading to high ΔD values, which is known for viscoelastic materials [52]. Samples with ΔD close to 0 behave solid-like. The measurements were performed with
130 the Q-Sense Analyser of Biolin Scientific (Sweden) [53, 54, 52]. The measurements were conducted with the QSoft software and analysed with the software Qtools of Biolin Scientific. SiO₂-coated sensors (product No. QS-QSX303) purchased from Quantum Design (Germany) were used as substrates. Through the use of the flow cell *in situ* cleaning was facilitated with 2 % Hellmanex, ethanol,
135 and water. By inverting the flow cell and thus placing the substrate on top of the solution, sedimentation onto the substrate could be avoided.

The measurement procedure was as follows: Initially, the flow cell was filled with water for calibration of the system to the ambient material used in the adsorption measurement. After the frequency stabilises and the crystal is smoothly
140 oscillating, the protein/salt mixture is pumped into the cell. 5 ml of mixture are pumped through the cell to allow sufficient solution exchange and then the pump is stopped for the duration of the adsorption process. After roughly 1h, water is

flushed through the cell to check for the reversibility of the adsorption process. Afterwards, the cleaning procedure in-situ or ex-situ is started. At least three
145 measurements per condition were performed to ensure reproducibility, stability, and accuracy of the trends found. The error bars reflect the standard deviation of those measurements. The systematic errors are substantially smaller than the statistical error.

The data was analysed with the Voigt viscoelastic model since the dissipation
150 D was > 0 [55, 54]. The used fitting parameters for the data analysis can be found in Tab. S1. For more information on the method and its analysis, the reader is referred to Refs. [56, 55, 54, 52, 48].

2.3.2. ATR-FTIR

ATR-FTIR allows structure determination of molecules adsorbed to a solid
155 interface. The infra-red beam hereby penetrates through the substrate and upon total internal reflection at the solid-liquid interface an evanescent wave is created, which has a penetration depth of a few microns into the bulk solution [57]. The information contained in the evanescent wave sheds light on the infra-red-active modes of the proteins adsorbed to the substrate in the dependence
160 on the wavenumber, which correspond to specific chemical bonds and can thus provide structural information on the protein adsorbed to the substrate [58]. For more information on the method, the reader is referred to Ref. [59].

The absorbance measurements were performed with the Thermo Nicolet iS50 Specac Gateway ATR insert and the software OMNIC was used for data collec-
165 tion [60]. The detection range was set to wave numbers from 1400 to 4000 cm^{-1} , yet, the area of interest was defined by the amide-I band (1600 to 1700 cm^{-1}). The number of scans was set to 294, the resolution to 4, the gain to 1 and the aperture to 8. The substrate used was a silicon block with a native oxide layer. Several background measurements were performed to account for the change in
170 environment over time (data not shown)(for more information see Ref. 48).

The evanescent wave penetrates through the substrate into the bulk solution. To estimate the intensity and contribution of the bulk proteins to the data

collected, we flushed the Si block after adsorption with water to compare the signal of the irreversibly adsorbed proteins with the signal of the protein bulk solution (data not shown). Even though this reduced the intensity, the overall shapes of the curves were the same, proving that the dominating signal came from the interface and that the protein structure was stable.

2.3.3. NR

Specular neutron reflectometry (NR) measurements were carried out using the PolRef time-of-flight reflectometer at the ISIS spallation source, Rutherford Appleton Laboratory (Oxfordshire, UK). A broad band neutron beam with wavelengths from 1 to 12 Å was used. The reflected intensity is measured as a function of the momentum transfer, Q_z ($Q_z = (4\pi \sin \theta)/\lambda$, where λ is wavelength and θ is the incident angle). The collimated neutron beam was reflected from the silicon–liquid interface at different glancing angles of $\theta = 0.6, 1.2$ and 2.3° in order to cover the desired Q -range.

Prior to use, the Si/SiO₂ substrates were cleaned in piranha solution 5:4:1 (water/sulphuric acid/hydrogen peroxide) and afterwards put for 10 min under UV-C light for ozone cleaning. Purpose-built liquid flow cells for analysis of the silicon–liquid interface (50 x 80 mm Si/SiO₂ substrate) were placed on top of a variable angle sample stage in the NR instrument and the inlet to the liquid cell was connected to a liquid chromatography pump (JASCO PU-4180), which allowed the automated exchange of the solution isotopic contrast within the (3 ml volume) solid–liquid sample cell. For each solution contrast change, a total of 10 ml solution (BLG/salt/H₂O(l) or BLG/salt/D₂O(l)) was pumped through the cell at a speed of 1.5 ml/min. The salt/protein mixture in D₂O(l) was pumped into the cell and after 20 min of equilibration the first neutron reflectivity measurement was started. We made use of the solvent contrast effect by exchanging D₂O(l) with H₂O(l).

Neutron data were analysed using the RasCAL2019 software package [61], which employs an optical matrix formalism (described in detail by Born and Wolf [62]) to fit layer models representing the interfacial out-of-plane structure.

In this approach, the interface is described as a series of slabs, each of which is characterised by its scattering length density (SLD), thickness, and roughness.

205 Contrast variation of $D_2O(l)$ and $H_2O(l)$ within one sample allows the simultaneous fit of the same sample in two solvents, which benefits the precision of the resulting fit parameters. For each condition, several datasets were simultaneously fitted: the bare substrate in $H_2O(l)$ and $D_2O(l)$, as well as the substrate in the presence of protein solution in both solvents. Only for data in regime

210 II, where the protein layer is assumed to be continuously growing, we omitted the protein in $H_2O(l)$ contrast (and only co-refined 3 contrasts). Interfacial roughness (or diffuse interfaces) was implemented in terms of an error function according to the approach by Nevot and Croce [63], but re-sampled in RasCAL in terms of thin slabs with zero roughness, thus allowing roughnesses, which are

215 of the order of the layer thickness. The reflectivity for an initial model based on known sample parameters, such as substrate, its oxide layer, and the solvent was calculated and compared with the experimental data. A least squares minimisation was used to adjust the fit parameters to reduce the differences between the model reflectivity and the data. In all cases, the simplest possible model

220 (i.e. least number of layers), which adequately described the data, was selected. Error analysis of the fitted parameters was carried out using Rascal’s Bayesian error algorithm [64]. The resulting plots contain fits and corresponding real space structure of the sample layer system, as well as 95 % confidence intervals (shown as shaded regions).

225 3. Results and discussion

3.1. Bulk phase behaviour

We investigate two salts, lanthanum chloride ($LaCl_3$) and lanthanum iodide (LaI_3), and their influence on the phase behaviour of BLG in $H_2O(l)$ and $D_2O(l)$ in Fig. 1a,b. Both salts in either solvent exhibit the same general trend showing

230 three regimes with boundaries at the salt concentrations c^* and c^{**} .

3.1.1. Phase diagrams

The general trend of the phase diagrams shown in Fig. 1 can be rationalised as follows. BLG is net negatively charged (-10 e) at neutral pH [65, 26]. This means that, without the addition of salt, repulsive forces are dominating and the samples of regime I are clear (see Fig. S1). The first phase boundary, defined by the specific salt concentration c^* , is reached, when the dominant interactions convert from repulsive to attractive due to multivalent cation binding and bridging [66, 67, 24]. Through the increase in salt concentration (c_s), protein aggregates start to form in regime II, which cause the solution to become turbid shown in Fig. S1. This can be observed and quantified either visually or by light transmittance measurements [49]. If c_s is further increased, the proteins undergo charge inversion from initially net negatively to net positively charged **due to multivalent cation binding and bridging**, resulting in decreased attractive interactions and the break-up of protein aggregates (clear solution in regime III, Fig. S1) [68, 69]. This behaviour is called re-entrant condensation (RC) and is defined by another boundary at c^{**} . In the present investigation, all samples in regime II and around the phase boundaries initially form aggregates and over time undergo liquid-liquid phase separation into a dilute and a dense liquid phase. Unlike some other proteins such as BSA, BLG initiates LLPS in a two-step process (Fig. 2), meaning first aggregates are formed and in a second step the system very slowly reorganises into a phase-separated solution. This behaviour is also found for other multivalent salts such as yttrium chloride (YCl_3) in combination with BLG [24]. In comparison with the phase diagram of BLG/ YCl_3 , the lanthanum salts induce a narrower regime II, which indicates weaker attractive forces induced by lanthanum(3+) ion (La^{3+}) being consistent with trends found for other globular proteins such as BSA [70, 71]. This can be rationalised to some degree with differences in surface charge density and polarisability of the individual cations [70, 71].

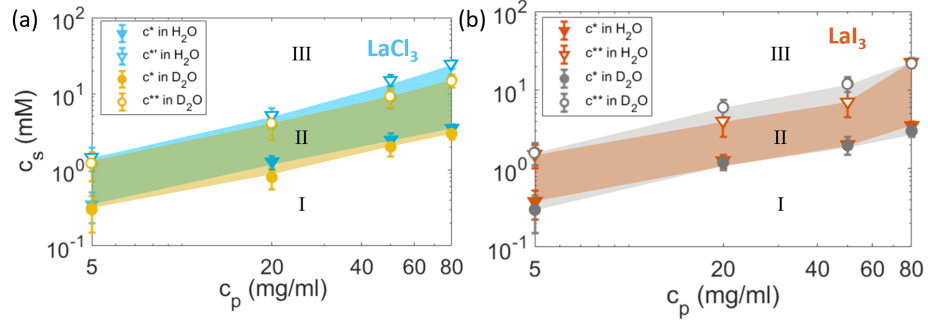


Figure 1: Phase diagrams. Phase behaviour of BLG (a) with LaCl_3 and (b) with LaI_3 in $\text{H}_2\text{O(l)}$ (triangles) and $\text{D}_2\text{O(l)}$ (circles), respectively. The solid markers define c^* , which separates regime I from regime II. The hollow markers define c^{**} , which separates regime II from regime III. The phase diagrams are nearly identical when comparing the different lanthanum salts and solvents. Note that the shift in phase boundaries with LaCl_3 between $\text{H}_2\text{O(l)}$ and $\text{D}_2\text{O(l)}$ might be introduced due to stock solution variations and fall within the statistical error of the measurements.

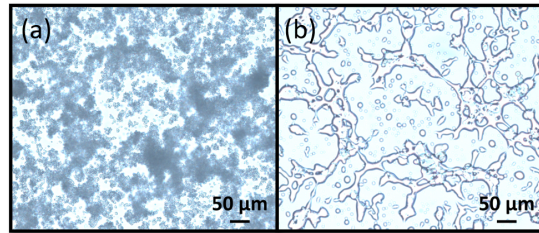


Figure 2: Two-step liquid-liquid phase separation. Microscopy images of a sample containing 20 mg/ml BLG and 2 mM LaI_3 in $\text{H}_2\text{O(l)}$. (a) Aggregation directly after preparation. (b) LLPS into a dilute and a dense phase after 1 h.

Table 1: Phase boundaries. This list contains the salt concentrations corresponding to the determined phase boundaries, c^* and c^{**} , of BLG at 5 mg/ml with LaCl_3 and LaI_3 in $\text{H}_2\text{O}(\text{l})$ and $\text{D}_2\text{O}(\text{l})$ by UV-vis transmittance measurements as shown in Fig. S2. **The errors listed in the table below depict the systematic and statistical variations of the phase boundaries resulting from protein batch variations, preparation imprecision, as well as protein and salt stalk solution variations.**

	LaCl_3		LaI_3	
Solvent	c^* (mM)	c^{**} (mM)	c^* (mM)	c^{**} (mM)
$\text{H}_2\text{O}(\text{l})$	0.3 ± 0.1	1.4 ± 0.3	0.3 ± 0.1	1.5 ± 0.3
$\text{D}_2\text{O}(\text{l})$	0.3 ± 0.1	1.2 ± 0.3	0.3 ± 0.1	1.4 ± 0.3

3.1.2. Bulk conditions for adsorption study

Our protein concentration of interest for the adsorption study is set to 5 mg/ml, which is high enough to observe the complete rich phase behaviour and to be physiologically relevant, but low enough to minimise the bulk signal, and thus, bulk scattering in the neutron reflectivity measurements. The phase behaviour at $c_p = 5$ mg/ml is illustrated in Fig. S2, which shows the measured transmittance runs via UV-vis spectroscopy since the determination of c^* and c^{**} by visual inspection at this protein concentration is not sufficiently precise. The determined values of c^* and c^{**} from Fig. S2 are listed in Tab. 1 (for more information see the materials and methods section). The phase diagrams of BLG, as well as the transmittance measurements, with the individual salts and solvents in Figs. 1 and S2 are quite similar to each other, yet small differences in trends can be seen. For LaI_3 , the phase boundaries occur at slightly higher c_s compared to LaCl_3 . The same can be observed for $\text{H}_2\text{O}(\text{l})$ compared to $\text{D}_2\text{O}(\text{l})$. These differences are within the statistical error of the measurements at 5 mg/ml. Note that pH can be excluded as a dominant driving force of the phase behaviour, see Fig. S3 [72].

3.1.3. Isotope effect in the bulk

Importantly, the known isotope effect of BSA [73], meaning significantly stronger attractive intermolecular forces in $D_2O(l)$ compared to $H_2O(l)$ and thus a strong shift in phase boundaries, is not observed for BLG. This is important
280 to mention since this means there are fundamental differences between BSA and BLG, despite both belonging to the group of net negatively charged globular proteins. In the case of BLG, we can make use of the solvent contrast for the neutron reflectivity measurements since the difference in phase behaviour is minimal between the two solvents (more details can be found in Section II.1).

285 The absence of the isotope effect in BLG may be rationalised by its secondary structure and amino acid sequence. It was found that β -sheets show little to no isotope substitution, thus no significant isotope effect, whereas α -helices contribute strongly to the isotope effect [74]. The helix formation substantially benefits, if a hydrophobic side chain is buried against the side of the helix since
290 it facilitates structural stability [75], which illustrates the correlation between hydrophobic interactions and the presence of α -helices. Hydrophobic interactions are enhanced in $D_2O(l)$ due to burying of hydrophobic groups leading to a stronger protein stability in $D_2O(l)$, [76, 77, 78, 79] and thus the combination of hydrophobic interactions and α -helices benefit the occurrence of a strong iso-
295 tope effect. Hence, a protein such as BSA being more hydrophobic than BLG (see Tab. 3) [80], as well as consisting predominantly of α -helices shows a strong isotope effect, whereas for BLG, the combination of fewer α -helices (15 %) and fewer hydrophobic interactions, as well as a strong contribution of β -sheets could explain the absence of a significant isotope effect.

300 3.1.4. Anion effect in the bulk

From the literature, it is clear that BLG binds only a few small anions such as chloride [81, 82]. The ability to bind small anions can be expressed in form of the binding index $\sum(NH^+)/[\sum(COO^-) - \sum(OH)]$, which is 4.6 for BLG, but 29 for BSA in comparison [83]. This is supported by Longsworth et al. [84], who
305 found anion binding lower by a factor of 2 for chloride and iodide to BLG, yet

the number of bound anions is higher for I^- than for Cl^- . In this context, it is useful to consider the conformation and structure of BLG. The number of free cationic vs anionic side chains in BLG is 48 (12.9 %) to 64 (17.9 %) [85], which illustrates the protein's stronger tendency to bind cations such as Ca^{2+} . In fact, BLG binds twice as many Ca^{2+} ions compared to BSA [86]. In addition, BLG tends to bind preferentially hydrophobic molecules via hydrophobic interactions [87, 9, 88, 89]. This is further supported by the absence of fixed anions in the protein's crystal structure [24]. Thus, we can assume that little to no anions bind to BLG, which supports the anion-independent phase behaviour observed in Fig. 1 and S2.

3.2. Protein adsorption

In this section, the adsorption behaviour of BLG ($c_p = 5$ mg/ml) at the solid-liquid interface is presented. For the characterisation of the adsorption layer, we use QCM-D, infra-red spectroscopy (ATR-FTIR), and neutron reflectivity (NR). Through the use of these complementary methods, we are able to gather information on the thickness, density, and hydration of the adsorption layer, as well as general trends introduced by the different bulk regimes. Silicon dioxide (SiO_2) is used as the substrate material and is net negatively charged and hydrophilic [90, 91].

3.2.1. Layer morphology and adsorption kinetics

Protein adsorption at the solid-liquid interface (SiO_2) is measured in real-time in a flow cell using a quartz-crystal microbalance with dissipation (QCM-D) and neutron reflectivity (NR). QCM-D allows to obtain insight into the adsorbed thickness d including the trapped water within in the layer and its viscoelastic properties [92, 93, 94, 56]. In addition, NR measurements at the solid-liquid interface are performed to provide information about the entire z-dependent density profile, i.e. thickness, density, roughness, hydration, and morphology of the adsorption layer. Fig. 5 shows an overview of the reflectivity curves of adsorbed BLG at different salt concentrations and salt types in $\text{D}_2\text{O}(\text{l})$.

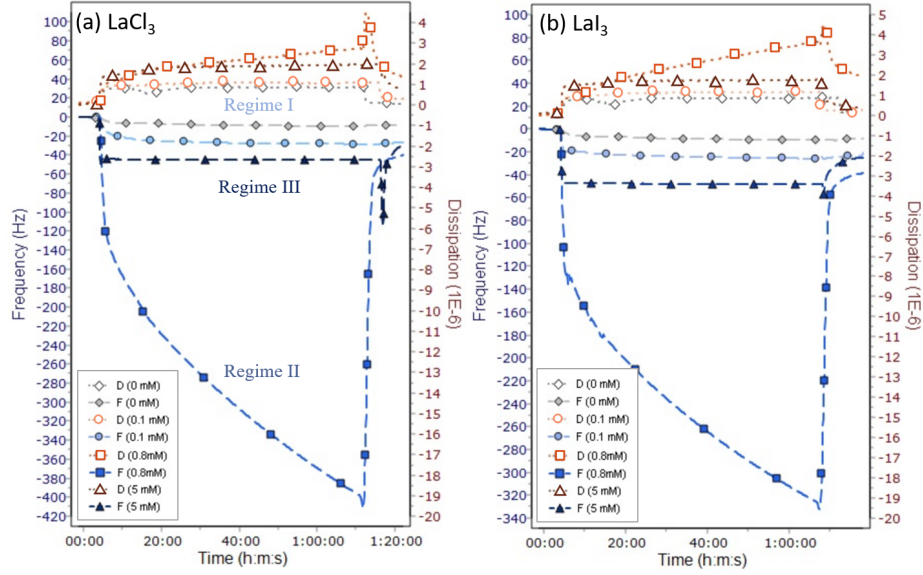


Figure 3: Raw QCM-D adsorption data. Frequency (blue) and dissipation (red) of the 9th overtone of BLG at 5 mg/ml in H₂O(l) without salt (diamonds), in regime I at 0.1 mM c_s (circles), in regime II at 0.8 mM c_s (squares) and in regime III at 5 mM c_s (triangles) adsorbed on a SiO₂-coated sensor in (a) with LaCl₃ and (b) LaI₃. The measurements are calibrated and started with the cell filled with H₂O(l) and after a few minutes the salt/water mixture is pumped into the cell inducing protein adsorption. After roughly 1 h, the cell is flushed with H₂O(l) to check for the reversibility of protein adsorption. Note that spikes in the raw data are induced by turning the pump on and off for solution exchange.

3.2.1.1. QCM-D measurements

From the raw QCM-D data, which consists of the measured frequency F and dissipation D , one can already deduce general trends and behaviours. Exemplary data is shown in Fig. 3 and S4 for BLG with LaCl_3 and LaI_3 in $\text{H}_2\text{O}(\text{l})$ and $\text{D}_2\text{O}(\text{l})$, respectively. The weakest adsorption (smallest ΔF) is measured without salt and the strongest adsorption occurs in regime II (highest ΔF) at 0.8 mM for both salts and solvents. The change in D varies from 1×10^{-6} to 4×10^{-6} . Since D is a measure for the viscoelastic properties, one can conclude that the protein layer formation is rather dense and stiff compared to e.g. BSA adsorbed on an interface [95, 96]. Upon rinsing, only in regime II, a significant amount of protein is flushed from the surface. Under all other conditions, most of the adsorption is irreversible, which implies strong protein-surface interactions. The adsorption process occurred on a time scale of seconds (which is not measurable by NR), except in regime II, where the layer continues to grow even after 1 h (Fig. 7).

By applying the viscoelastic Kelvin-Voigt model [54, 97, 98], the averaged adsorbed protein layer thickness d over a cross-section of the substrate is calculated (details in the materials and methods section) and shown in Fig. 4. Without salt, very little adsorption is observed ($d_{\text{LaCl}_3} = 1.8 \pm 0.9$ nm) in Fig. 4a. Adding trivalent salt causes an enhancement in adsorption. At $c_s = 0.1$ mM (regime I), a slight increase to $d_{\text{LaCl}_3} = 6.9 \pm 2.6$ nm can be seen in $\text{H}_2\text{O}(\text{l})$. By further increasing c_s to 0.8 mM (regime II), thus crossing the first bulk phase boundary, strongly enhanced adsorption ($d_{\text{LaCl}_3} = 60.1 \pm 11.2$ nm) is observed. This is in good agreement with enhanced adsorption found for BSA with multivalent ions [96]. This adsorption trend can be explained with the ion-activated-attractive protein adsorption model established in this context [95]. In a previous publication [96], we established that this enhanced adsorption can actually be discussed in terms of a wetting transition, i.e. the divergent layer represents a wetting layer, triggered by bulk instability due to LLPS formation. From the bulk phase behaviour, we know that BLG also undergoes LLPS formation in a two-step process in the conditions studied, which gives rise to

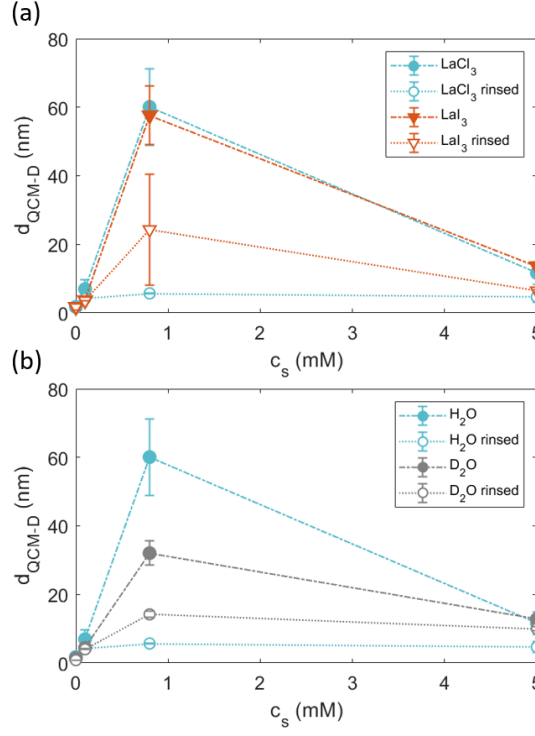


Figure 4: Solid-liquid BLG adsorption. Adsorbed layer thickness d calculated with a viscoelastic model from the QCM-D data for 5 mg/ml BLG on SiO_2 at room temperature. (a) Influence of anion type on BLG adsorption with LaCl_3 (blue) and LaI_3 (orange) in $\text{H}_2\text{O}(\text{l})$. (b) Influence of solvent type on BLG adsorption in the presence of LaCl_3 in $\text{D}_2\text{O}(\text{l})$ (grey) and $\text{H}_2\text{O}(\text{l})$ (blue). The solid markers are samples in the salt/protein mixtures and the hollow markers label the samples after flushing the cell with the respective solvent to check the reversibility of the adsorption process. The dashed lines are guides to the eye.

strongly increased adsorption i.e. wetting layer illustrated in Fig. 3. At high c_s (5 mM, regime III), d_{LaCl_3} decreases to 11.6 ± 3.3 nm showing re-entrant adsorption probably caused by an overcharging effect of the substrate at high c_s , which leads to stronger interface-protein repulsion.

370 For both salts in Fig. 4a, the adsorption curves lie within the error bars on top of each other, meaning the different anions (Cl^- vs I^-) do not cause observable changes. This is in accordance with their similar protein bulk phase behaviour for BLG shown in Fig. 9 (note that these effects are completely different for BSA [71, 48]).

375 Concerning the isotope effect (solvent exchange), the raw data can be found in Fig. S4 and the analysed data is shown in Fig. 4b. The $\text{D}_2\text{O}(\text{l})$ data of LaCl_3 follows the same trend as the $\text{H}_2\text{O}(\text{l})$ data with little adsorption in regime I, enhanced adsorption in regime II, and re-entrant adsorption in regime III. Yet in regime II, a solvent effect is observed, which was not present in the bulk
380 behaviour. Here, adsorption was decreased by a factor of ≈ 2 for $\text{D}_2\text{O}(\text{l})$. In regime II, the dominant interactions are attractive. One explanation could be that deuterium introduces stronger deuterium bonds than hydrogen bonds [99], which leads to stronger solvent-solvent interactions in $\text{D}_2\text{O}(\text{l})$, as well as stronger solvent-protein interactions [76], which diminish (or compete with) the
385 attractive protein-surface interactions. In addition, the protein stability and rigidity in $\text{D}_2\text{O}(\text{l})$ [77] may hinder excessive adsorption and rather keeps the proteins in the bulk solution. Nevertheless, the differences in regime I and III are marginal, and so solvent contrast techniques could be used for NR.

3.2.1.2. NR measurements

390 The NR measurements (Fig. 5) are in good agreement with the QCM-D and ATR-FTIR data (cf. Section II.2). By applying a one-layer model, we could fit the SLD of our sample in Fig. 5, from which it is possible to extract the adsorbed protein layer thickness d_{NR} , and additional structural features such as the adsorption layer roughness σ and the hydration of the adsorbed layer. All
395 extracted parameters and their 95 % confidence intervals are listed in Tab. 2. BLG is a rather small protein ($R_{\text{H}} = 2.35$ nm) and has a high charge density,

Table 2: Results of fitting the NR reflectivity data of BLG at 5 mg/ml with LaCl_3 and LaI_3 obtained by co-refining NR data in $\text{H}_2\text{O}(\text{l})$ and $\text{D}_2\text{O}(\text{l})$. d_{NR} defines the adsorbed protein layer thickness, σ defines the layer roughness and 'Hydr.' the hydration of the layer. Sub- and superscript values are parameter limits at the 95 % confidence interval (CI). Data and fits with Bayesian error analysis are shown in Fig. 6 and the Supporting Material (Figs. S5 and S6).

	LaCl_3 (\pm 95 % CI)			LaI_3 (\pm 95 % CI)		
c_s	d_{NR} (nm)	σ (nm)	Hydr. (%)	d_{NR} (nm)	σ (nm)	Hydr. (%)
no salt	2.8 $^{4.5}_{0.1}$	1.4 $^{2.2}_{0.9}$	91 $^{99}_{79}$	2.8 $^{4.5}_{0.1}$	1.4 $^{2.2}_{0.9}$	91 $^{99}_{79}$
0.1 mM (I)	3.8 $^{4.5}_{3.1}$	0.9 $^{1.4}_{0.3}$	49 $^{70}_{35}$	3.9 $^{4.8}_{3.1}$	1.2 $^{1.8}_{0.3}$	51 $^{70}_{37}$
0.8 mM (II)	19.8 $^{24.0}_{15.5}$	8.1 $^{11.8}_{4.4}$	43 $^{54}_{33}$	18.9 $^{20.3}_{13.0}$	4.5 $^{7.9}_{2.7}$	53 $^{58}_{44}$
5 mM (III)	6.1 $^{6.9}_{5.2}$	1.6 $^{2.5}_{1.0}$	36 $^{59}_{16}$	6.5 $^{7.2}_{5.8}$	1.6 $^{2.5}_{1.1}$	35 $^{56}_{14}$

which leads to strong repulsive forces. Thus, without salt, the NR fits show a highly hydrated (low volume fraction) protein layer with a thickness of 2.8 nm and a hydration of 91 %. At low c_s , a small feature is visible at $Q_z = 0.1 \text{ \AA}^{-1}$,
400 indicating the formation of a distinct and denser layer of 3.8 nm with a hydration of 49 %. In both cases (no salt and 0.1 mM), a two-layer model was also tested, but discarded, since the error analysis did not justify the assumption of two distinct layers. Thus, in regime I, BLG forms (less than) a monolayer, the density (or volume fraction) of which increases, as salt is added. The roughness
405 of the layer at 0.1 mM salt concentration is 1.2 nm, which indicates a rather ordered layer.

In regime II, enhanced adsorption is observable (see Fig. 5 and 7). **As the adsorbed layer is continually growing over several hours in regime II, we fitted only the D_2O data set which was measured immediately after injection. The**
410 **NR data yield a layer thickness of approximately 20.0 nm (see Tab. 2 for exact figures and error bars) with a hydration of 43-53 %. The layer roughness is rather high (8.1 nm), suggesting a much more inhomogeneous layer, possibly caused by the adsorption of aggregates from solution, rather than growth arising from adsorption of individual proteins, which is consistent with a wetting transition**

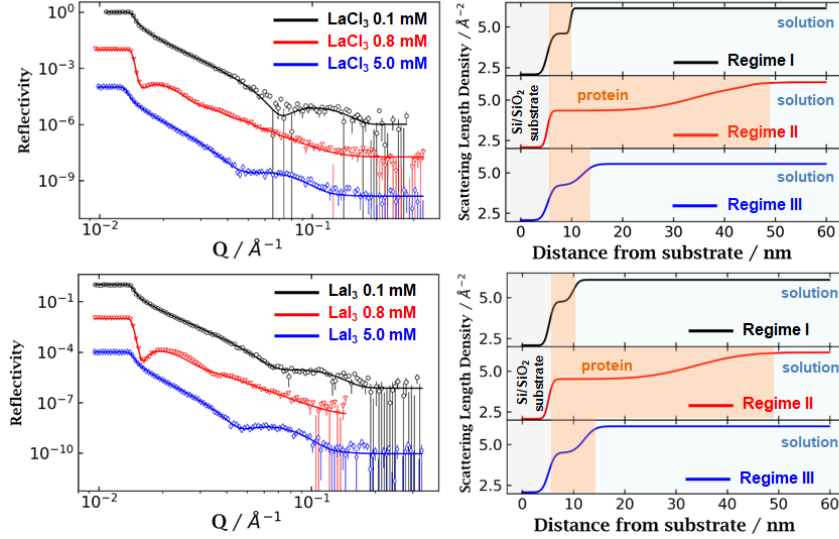


Figure 5: Neutron reflectivity data in $D_2O(l)$ (right) and derived scattering length density (real space) profiles (left) of 5 mg/ml **BLG** adsorbed to SiO_2 in the presence of (a) $LaCl_3$ and (b) LaI_3 . The shaded areas in the SLD plots indicate the regions of substrate (light grey), protein layer (orange) and solvent (light blue). Note that the $H_2O(l)$ reflectivity curves are not shown for better clarity, but can be found in the Fig. 6 and in the Supporting Material (Figs. S5 and S6).

[96] and the consequential morphology change. It is interesting to note that the hydration of the protein layer does not suggest any significant denaturation of protein at the interface, which is also in agreement with the ATR-FTIR analysis (shown in the next Section II.2). In agreement with QCM-D and ATR-FTIR, we detect re-entrant adsorption and the diverging thickness in regime II.

In absolute numbers, the overall trend is very clear. There was nearly no difference between protein adsorption in the presence of $LaCl_3$ and LaI_3 . The thicker the adsorption layer becomes, the rougher it becomes, while the hydration is around 50 % for regimes I and II, but drops to about 35 % in regime III (with larger uncertainty). This reduced hydration is below that of a minimally solvated protein layer and potentially suggests some denaturation. This, however, was a small effect and could not be confirmed in the ATR-FTIR mea-

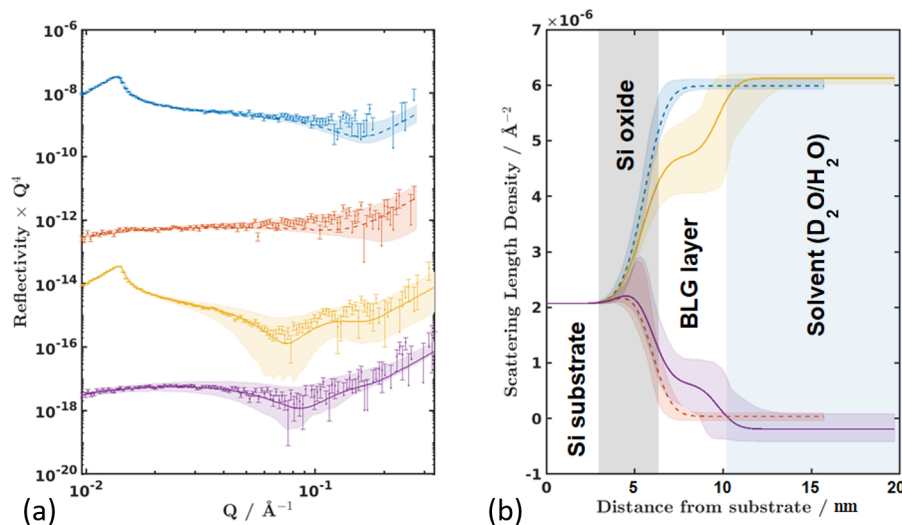


Figure 6: Bayesian error analysis. Model fit showing 95 % confidence intervals (shaded regions) of (a) the generated reflectivity curves and (b) the resulting scattering length density profiles. The example shows a typical co-refined fit of the bare substrate, i.e. without protein (blue and red,dashed) and regime I, i.e. 0.1 mM LaCl₃, (yellow and purple, solid), in D₂O(l) and H₂O(l), respectively.

surements.

A hydration of around 50 % indicates that the protein layer is densely packed. This might be rationalised with BLG naturally occurring as a dimer [100], as
 430 well as its ability to crystallise. Sufficiently close proximity between proteins is required to start the nucleation process.

In order to assess the accuracy and precision of the created fitting model, we performed a Bayesian error analysis. The error intervals given in Tab. 2 are obtained from this analysis and denote 95 % confidence intervals. An example
 435 is shown in Fig. 6 of 5 mg/ml BLG with no salt and 0.1 mM LaCl₃. The shaded areas depict the possible fit and real space profile ranges within the 95 % confidence interval. Although the 95 % confidence interval is broader than usual, the adsorption trend and structural changes can be clearly determined.

Here, one can see the benefit of using the solvent contrast of D₂O(l) and

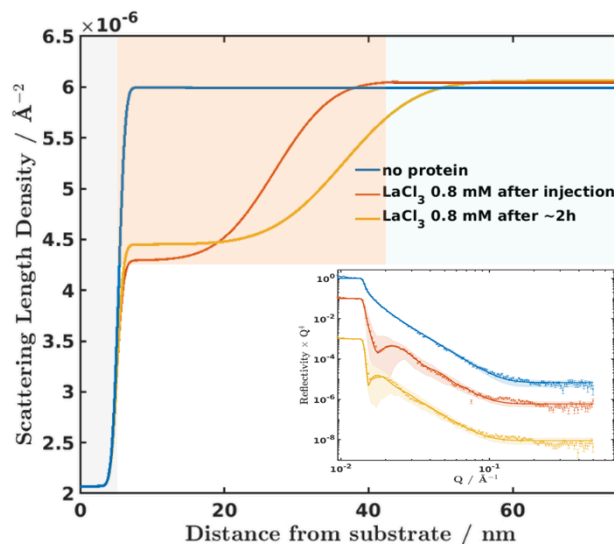


Figure 7: Wetting layer growth in regime II. Time-dependent reflectivity curves of 5 mg/ml BLG at 0.8 mM LaCl_3 in $\text{D}_2\text{O}(\text{l})$. The shaded areas in the SLD plots indicate the regions of substrate (light grey), protein layer (orange) and solvent (light blue). The adsorption layer continuously kept on growing in thickness and in density (red: after injection, blue: after 2 h). The fitted thicknesses were: 19.8 nm [15.5, 24.0] 95% CI after injection and 28.8 nm [24.7, 32.7] 95% CI after 2h.

440 $\text{H}_2\text{O}(\text{l})$ due to the different shape of the reflectivity curve and $\text{D}_2\text{O}(\text{l})$ having a critical edge. This is based on their different SLDs and allows tailored data analysis. Note that the QCM-D data shows reduced protein adsorption in regime II in $\text{D}_2\text{O}(\text{l})$ compared to $\text{H}_2\text{O}(\text{l})$. For this reason and due to the fact that the protein layer was increasing relatively quickly, for the NR measurements in
 445 regime II only the $\text{D}_2\text{O}(\text{l})$ data set (and the $\text{D}_2\text{O}(\text{l})$ and $\text{H}_2\text{O}(\text{l})$ data of the bare substrate) were used for fitting. However, due to the strongly enhanced adsorption in both solvents compared to the other regimes does not detract from the overall adsorption trend.

Based on the QCM-D results, which show a continuing growth in regime
 450 II even after more than 1 h (Fig. 3), we followed the adsorption kinetics of the LaCl_3 sample in regime II for more than 2 h (Fig. 7). We observe an enhanced and growing adsorption layer of almost constant density and increasing

roughness. As can be seen, the data in D2O(l) shows a fringe and a peak at relatively low Q , indicating the presence of a thick layer. The peak position
455 shifts to lower Q after 2-3 h, which relates to an increase in thickness. The fitted thicknesses were 19.8 nm [15.5, 24.0] 95 % CI after injection and 28.8 nm [24.7, 32.7] 95 % CI after 2-3 h. This is consistent with previous findings in BSA showing a wetting transition at the interface for samples in the LLPS regime [96] and emphasising its universality.

460 3.2.2. Layer stability via ATR-FTIR

Attenuated total reflection Fourier-transform-infra-red spectroscopy (ATR-FTIR) was used to study the layer stability and structural arrangement after protein adsorption on the solid-liquid SiO_2 interface. IR absorbance measurements are able to provide insight into the secondary structure, which can be
465 inferred from the amide-I band at 1600 to 1700 cm^{-1} . In Fig. 8, the ATR-FTIR spectra of BLG with different concentrations of LaCl_3 and LaI_3 in $\text{H}_2\text{O}(\text{l})$ are plotted. The peak maxima at 1632 cm^{-1} correlate with the presence of β -sheets, which make up 54 % of the BLG structure [101, 102]. We can thus conclude that the main protein structure seems to be largely intact and is not strongly affected
470 by the addition of multivalent salts or the adsorption to a solid interface.

The LaCl_3 and LaI_3 data in Fig. 8 show the same intensities in absorbance and curve shapes in the individual regimes. No salt-dependent structural changes can be found. Another interesting observation is the change in absorbance over the different regimes, which does directly correlate with the amount of proteins
475 adsorbed to the interface. Again, re-entrant adsorption (red curve) and enhanced adsorption (black curve) in regime II can be observed, which reflect the findings of the QCM-D data in Fig. 4a and the NR data in Tab. 2.

4. Discussion on differences between BSA and BLG

This investigation provides insight into the dependence of BLG on different
480 parameters, which guide its bulk phase behaviour and adsorption behaviour. In order to understand better what is protein-specific, we compare BLG to BSA,

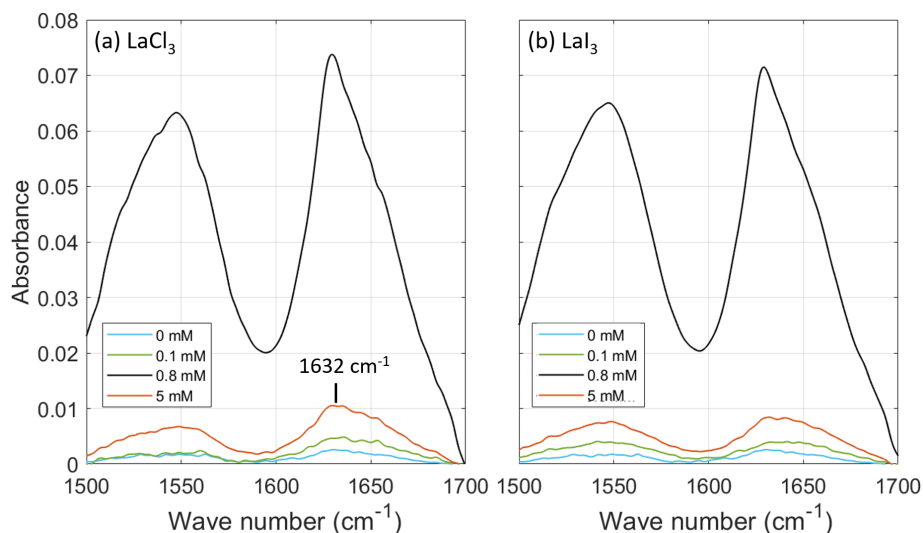


Figure 8: Interfacial structure stability of BLG. ATR-FTIR absorbance measurements of BLG at 5 mg/ml in $\text{H}_2\text{O}(\text{l})$ with (a) LaCl_3 and (b) LaI_3 at different c_s adsorbed on SiO_2 are presented. The shapes of the curves are similar to each other under all conditions meaning the same intact protein structure can be assumed.

which is the most commonly used protein for adsorption studies. In this section, we summarise and discuss certain protein-specific behaviours found (Tab. 4) and try to relate those to specific protein properties listed in Tab. 3. We note, though, that of course the resulting behaviour is always the result of a complex interplay of several factors, so that typically there is no simple correspondence between a certain effect and only one parameter.

First, we focus on similarities and differences in the *bulk* phase behaviour of BSA and BLG:

- **Role of cations.** Our group investigated two multivalent cations, La^{3+} and Y^{3+} (yttrium(3+) ion), and their role on the BSA and BLG phase behaviour. In a previous publication, Matsarskaia et al. [70] established the influence of La^{3+} , Y^{3+} , and Ho^{3+} (holmium(3+) ion) on the BSA phase behaviour and Zhang et al.[24] on the phase behaviour of BLG with YCl_3 . Depending on the cation size, thus its surface charge density and

Table 3: Protein properties. Relevant parameters, which influence the possible interactions of BSA and BLG.

Parameter	BLG	BSA
Hydrodynamic radius at pH=7 [103, 104] R_H (nm)	2.35	3.5
Molecular weight (monomer) [105, 104] M_w (kDa)	18.3	66
Isoelectric point [65, 106]	5.2	4.6
Net charge at pH=7 [65, 106] (e^-)	-10	-10
Gibbs free energy of transfer from water [80] ΔG (kcal/mol)	-1.7	-5.1
Extinction coefficient [107] $\epsilon_1^{279 \text{ nm}}$ (ml/(mg·cm))	0.96	0.667
Anion binding index [83] $\sum(\text{NH}^+)/[\sum(\text{COO}^-) - \sum(\text{OH})]$	4.6	29
Secondary structure [102, 108]	$\alpha \sim 15\%$	$\alpha \sim 66\%$
	$\beta \sim 54\%$	$\beta \sim 21\%$
Natural configuration at pH=7 [32, 109]	dimer	monomer

polarisability, its influence on the dominant bulk interactions can be estimated. The higher the surface charge density of the cation, the stronger protein-protein forces are expected, but there are also non-trivalent entropic contributions, which are difficult to estimate [110, 111].

- Liquid-liquid phase separation.** We find that LLPS forms in one step with BSA and in two steps with BLG (first aggregates in Fig. 2a). LLPS is temperature-driven. The different behaviours are influenced by entropy and enthalpy of mixing and de-mixing [112], which results in a lower critical solution temperature (LCST) for BSA [66] and an upper critical solution temperature (UCST) for BLG solutions under the conditions studied [24]. The only exception is BSA with LaCl_3 , in which no LLPS was found at our conditions studied. Here, the attractive forces are the weakest compared to the other systems studied and do not become strong enough to induce LLPS, which is also reflected in the phase boundaries at lower c_s .
- Role of solvent (isotope).** We observe a strong isotope effect for BSA in

bulk solution, which was also shown in a previous investigation by Braun et al. [100], and the absence of a significant isotope effect for BLG illustrated in Fig. 1. The strength of solvent-solvent hydrogen bonds in $D_2O(l)$ is increased compared to $H_2O(l)$ [113], which leads to enhanced hydrophobic interactions within the protein stabilising and stiffening the protein structure [76, 77, 78, 79]. The hydrophobicity of a protein can be determined and expressed in multiple ways [114, 115]. One way is the Gibbs free energy of transfer from water, which is a direct method and was determined for BSA and BLG by Pérez-Fuentes et al. [80] (see Tab. 3). According to that, BSA is more hydrophobic than BLG [116, 117, 88, 118] meaning BSA will feel a stronger impact of $D_2O(l)$. The hydrophobicity of a protein depends on its amino acid sequence, as well as its secondary structure. For α -helix formation, hydrophobic amino acids are essential, since those provide stabilisation to the structure [75]. Thus, the presence and general nature of α -helices contributes to the hydrophobicity of a protein and consequently to the amide isotope effect. In contrast, β -sheets show no isotope substitution and consequently no isotope effect [74]. BLG belonging to the protein class of all- β , therefore, will not undergo D/H isotope substitution for most of its structure compared to BSA belonging to the class of all- α (see Tab. 3) [119]. Thus, the difference between a strong isotope effect for BSA and its absence in BLG systems can be rationalised with its secondary structure/amino acid sequence and hydrophobicity as illustrated in Fig. 9.

- **Role of anions.** There seems to be a fundamental difference in the ability to bind anions between BSA and BLG. We find that for BSA the anions impacted the BSA bulk phase behaviour differently depending on the anion type. The protein-salt interaction strength and contribution of anions to the phase boundaries increases from $Cl^- < NO_3^- < I^-$ [48], whereas for BLG all anions induce the same behaviour as shown in Fig. 1. The anion behaviour with BSA is in good agreement with literature from Carr et al.

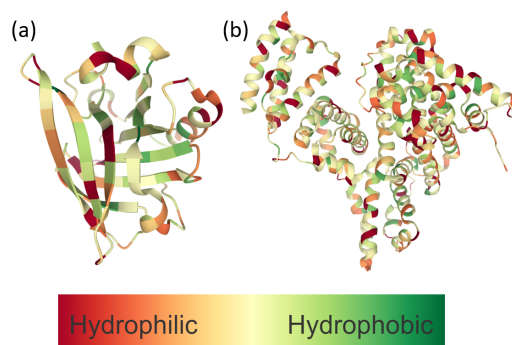


Figure 9: Hydrophobicity and 3D structure of proteins. These protein images of (a) BLG (PDB ID: 3PH6) [24] and (b) BSA (PDB ID: 4F5S) [120] are created with Mol* [121] on the RCSB PDB website (rcsb.org). The differences in secondary structure (α -helices and β -sheets) are prominent (see also Tab. 3) and the colour code illustrates the hydrophobicity of different amino acids based on the work of Wimley and White [122]. Note that for better clarity BLG is illustrated only as a monomer.

[123] and Longsworth et al. [84], which found that the number of anions bound per mole protein increases from $\text{Cl}^- < \text{Br}^- < \text{NO}_3^- < \text{I}^- = \text{CNS}^-$. Carr et al. [86] determined that 8 Cl^- anions are bound to BSA at pH 5, but 12 I^- ions. This effectiveness of specific binding of anions is similar for BLG [84], but reduced by a factor of 2 according to Longsworth et al. [84]. The parameter 'anion binding index' coined by Klotz et al. [83] illustrates the protein's affinity to bind anions. The anion binding index is 29 for **bovine** serum albumin and 4.6 for β -lactoglobulin (Tab. 3). This is further supported by Tanford et al. [82] and the number of chloride ions bound by each protein. Chloride, in general, has a passive role [82, 81, 124] and is also not traceable in the BLG crystal structure [125, 24]. A recent study by Maier et al. [125] evaluated the surface coverage of cations on proteins of protein crystals after cation binding (here: Y^{3+}). In BLG, 30 % of its surface is covered with cations in comparison to only 15 % coverage for HSA, meaning less space is available for anions to bind to BLG. (Note that while HSA is a different protein than BSA, their structures are to

roughly 70 % identical, thus it is fair to assume that they should show similar surface coverage of bound cations.) Another explanation for the stronger anion binding of BSA might be the difference in binding mechanisms. BSA has a high affinity for anionic binding [126], whereas BLG prefers to bind hydrophobic molecules via hydrophobic interactions [87].

- **Re-entrant condensation.** Re-entrant condensation is driven by protein charge inversion and, beyond a certain concentration, consequently decreasing the attractive protein-protein interactions, which cause the cation-bridged protein clusters to break up [106]. In the presence of chloride salts, BSA and BLG undergo re-entrant condensation, as well as in the presence of iodide salts for BLG (shown in Fig. 1). For BSA with iodide salts, the samples stay in regime II upon increasing c_s and do not redissolve, i.e. do not reach regime III (Fig. 1a,b of Ref. 48). In the systems with chloride salts, chloride has a passive role [124] and thus cations have the dominant role. In the system of BLG with iodide salts, BLG has in general a low anion binding affinity [83, 84], thus providing the mechanism for the occurrence of re-entrant condensation driven by multivalent cations. This behaviour changes for BSA with iodide salts. Iodide has a prominent role due to its protein stabilising role [127, 128], stronger binding to BSA [129], and a higher quantity bound to BSA [84, 123] than chloride. Additionally, an interplay between hydrophobic and charged amino acids improves anion binding to BSA [126, 130]. Thus, iodide induces stronger attractive protein-protein interactions and might facilitate anion-mediated protein cluster formation, which hinders re-entrant condensation.

Next, we focus on similarities and differences in protein *adsorption* of BSA and BLG on negatively charged and hydrophilic SiO_2 :

- **Role of cation and anions.** The role of ions on the protein adsorption behaviour is reflected by its bulk properties. The stronger interactions an ion induces in bulk, the stronger is its effect on protein adsorption, in the

sense that it enhances adsorption on SiO_2 . One exception is BSA/ YI_3 , in which the combination of a strong cation with a strong anion seems to hinder each other.

- 590 • **Adsorption without salt.** Numerous studies have shown that the adsorbed thickness of BLG without salt is reduced compared to BSA [131, 132, 103], which is consistent with our findings. BLG has a smaller size (Tab. 3) than BSA and a higher surface charge density, which induces strong repulsion in a system with negatively charge surfaces (proteins and
595 substrate) and thus limits surface adsorption.
- **Re-entrant adsorption.** The non-monotonic behaviour in adsorption at high c_s , i.e. decrease in adsorbed amount, can be observed for both proteins (Fig. 4 and 5 and in Ref. 48) and all salts in either solvent. Thus, we can conclude that it is related to the surface properties and not
600 only to the bulk behaviour e.g. re-entrant condensation, which is absent for BSA with iodide salts in Ref. 48. Due to surface properties being hydrophilic and net negatively charged, anion binding is hindered and solely the cations and solvent are interacting with the surface. In the vicinity of the substrate (substrate and proteins are initially negatively
605 charged), local charge inversion due to multivalent cation binding (i.e. stronger protein-interface repulsion) at high c_s can be induced leading to re-entrant adsorption independent of the bulk properties.
- **Enhanced adsorption/Wetting transition.** In regime II, attractive interactions dominate the system, which induces enhanced adsorption
610 compared to regime I and III in all systems studied (see Fig. 3 and 7). The maximum adsorbed amount d is limited by the strength of the cation/anion in the system and/or LLPS formation. In systems with LLPS, we observe continuous adsorption of proteins and the formation of a wetting layer at the bulk instability [96]. The general mechanism is explained in Ref. 96. This wetting transition discussed in Ref. 95, 96, 48
615 appears to be general, yet, the morphology of this wetting layer differed

Table 4: Protein phase and adsorption behaviour. Properties and effects of BLG and BSA established in this work and previous studies of our group [48, 96, 95]. While the two proteins can show either temperature dependency, LCST and UCST, depending on the position in the phase diagram [133], they show the behaviour listed below under the conditions studied.

Protein behaviour	BLG	BSA
LLPS	Two-step	One-step
Re-entrant condensation	✓	✓ / X
Crystallisation	✓	X
Temperature dependency [134, 24, 66]	UCST	LCST
Isotope effect	X	✓
Anion effect	X	✓
Cation effect	✓	✓
Adsorption without salt	✓	✓
Re-entrant adsorption	✓	✓
Wetting transition	✓	✓

for BSA and BLG. In BSA, the wetting layer was diffuse with a high content of associated water trapped within [96] and in BLG, a densely packed layer formation can be observed (only 50 % hydration in Tab. 2). This difference could be speculated to be, under favourable conditions, the basis for the nucleation of protein crystals at interfaces in BLG systems and the absence of those in BSA systems, as well one has to bear in mind that BLG in its natural state forms dimers at the given pH (pH = 7) [100].

5. Conclusions

In this study, we focus on the role of anions and solvents on the BLG behaviour in the bulk and at interfaces. We find that BLG is influenced **much** less by the anion type or the solvent than **other globular proteins such as BSA. Neither the bulk (protein-protein) interactions, nor the interface (protein-substrate)**

interactions, were significantly influenced by the change in anion or solvent type.

630 **The solvent insensitivity** can be rationalised with its secondary structure (mainly β -sheets) and the properties of its amino acids. **The anion insensitivity** is consistent with literature showing a decreased affinity of BLG to bind anions in general compared to BSA [83, 84] **since BLG prefers the binding of hydrophobic ligands [87]**. All phase diagrams established show re-entrant condensation and LLPS, 635 which is induced by binding and bridging of multivalent cations. Through the addition of multivalent salts to the protein solution, protein adsorption increased at the interface up to a critical c_s , after which re-entrant adsorption occurred. The enhanced adsorption in regime II has been previously established for BSA [96] and, when combined with this work, illustrates the universality of a "wetting" transition at a bulk instability induced by LLPS formation. In addition, 640 we find systematic differences between BSA and BLG and correlate those to their specific structure and properties. **These findings illustrate universal behaviours of globular, net negatively charge proteins at neutral pH, which could enable the controlled manipulation of protein-protein and protein-substrate interactions in complex systems.** In the future, the combination of neutron and 645 X-ray reflectivity may pave the way to study the transition from adsorption to crystallisation, i.e. nucleation at interfaces.

CRediT authorship contribution statement

Madeleine R. Fries: Conceptualization, Methodology, Validation, Formal analysis, Investigation, Writing - Original draft preparation, Visualisation; 650 **Maximilian W. A. Skoda:** Conceptualization, Methodology, Validation, Software, Formal analysis, Investigation, Resources, Data Curation, Writing, Visualisation; **Nina F. Conzelmann:** Formal analysis, Investigation; **Robert M. J. Jacobs:** Conceptualization, Methodology, Formal analysis, Investigation, Data Curation; 655 **Ralph Maier:** Formal analysis, Investigation; **Niels Scheffczyk:** Formal analysis, Investigation; **Fajun Zhang:** Validation, Resources, Supervision; **Frank Schreiber:** Conceptualization, Project adminis-

tration, Funding acquisition, Resources, Data Curation, Writing, Supervision.

Declaration of Competing Interest

660 The authors declare that they have no known competing financial interests or personal relationships that could have appeared to influence the work reported in this paper.

Data availability

The experimental data are available from the corresponding author on rea-
665 sonable request.

Acknowledgements

The authors thank Resul Akyüz and Alexander Krauth for their assistance in the experiments and the ISIS Biolab for granting us excess to the ATR-FTIR. Neutron beam time on the POLREF reflectometer was awarded by the ISIS Fa-
670 cility, experiment number RB1910571 (DOI: 10.5286/ISIS.E.RB1910571). Funding by Deutsche Forschungsgemeinschaft and instrument grant by Tübingen University/LISA⁺ is gratefully acknowledged.

Appendix A. Supporting Material

Supplementary data to this article can be found online at XXX.

675 References

- [1] P. J. Moughan, Digestion and absorption of proteins and peptides, in: Designing functional foods, Woodhead Publishing, 2009, pp. 148–170.
- [2] S. Bilsborough, N. Mann, A review of issues of dietary protein intake in humans, International Journal of Sport Nutrition and Exercise Metabolism
680 16 (2) (2006) 129–152.

- [3] G. H. Anderson, S. E. Moore, Dietary proteins in the regulation of food intake and body weight in humans, *The Journal of Nutrition* 134 (4) (2004) 974S–979S.
- [4] Y. Guigoz, Dietary proteins in humans: basic aspects and consumption in Switzerland, *International Journal for Vitamin and Nutrition Research* 81 (2-3) (2011) 87–100.
- [5] J. Halkjaer, A. Olsen, L. J. Bjerregaard, G. Deharveng, A. Tjønneland, A. A. Welch, F. L. Crowe, E. Wirfält, V. Hellstrom, M. Niravong, et al., Intake of total, animal and plant proteins, and their food sources in 10 countries in the european prospective investigation into cancer and nutrition, *European Journal of Clinical Nutrition* 63 (4) (2009) S16–S36.
- [6] G. Kontopidis, C. Holt, L. Sawyer, Invited review: β -lactoglobulin: binding properties, structure, and function, *Journal of Dairy Science* 87 (4) (2004) 785–796.
- [7] M. D. Pérez, M. Calvo, Interaction of β -lactoglobulin with retinol and fatty acids and its role as a possible biological function for this protein: a review, *Journal of Dairy Science* 78 (5) (1995) 978–988.
- [8] Q. Wang, J. C. Allen, H. E. Swaisgood, Binding of vitamin D and cholesterol to β -lactoglobulin, *Journal of Dairy Science* 80 (6) (1997) 1054–1059.
- [9] S. Le Maux, S. Bouhallab, L. Giblin, A. Brodkorb, T. Croguennec, Bovine β -lactoglobulin/fatty acid complexes: binding, structural, and biological properties, *Dairy Science & Technology* 94 (5) (2014) 409–426.
- [10] A. Mansouri, J.-L. Guéant, J. Capiamont, P. Pelosi, P. Nabet, T. Haertlé, Plasma membrane receptor for beta-lactoglobulin and retinol-binding protein in murine hybridomas, *Biofactors* 7 (4) (1998) 287–298.
- [11] H. C. Liu, W.-L. Chen, S. J. T. Mao, Antioxidant nature of bovine milk β -lactoglobulin, *Journal of Dairy Science* 90 (2) (2007) 547–555.

- [12] G. Brignon, A. Chtourou, B. Ribadeau-Dumas, Does β -lactoglobulin occur in human milk?, *Journal of Dairy Research* 52 (2) (1985) 249–254.
- 710 [13] K.-M. Järvinen, P. Chatchatee, L. Bardina, K. Beyer, H. A. Sampson, IgE and IgG binding epitopes on α -lactalbumin and β -lactoglobulin in cow's milk allergy, *International Archives of Allergy and Immunology* 126 (2) (2001) 111–118.
- 715 [14] Z. Teng, Y. Luo, Y. Li, Q. Wang, Cationic beta-lactoglobulin nanoparticles as a bioavailability enhancer: effect of surface properties and size on the transport and delivery in vitro, *Food Chemistry* 204 (2016) 391–399.
- [15] Z. Teng, R. Xu, Q. Wang, Beta-lactoglobulin-based encapsulating systems as emerging bioavailability enhancers for nutraceuticals: a review, *Rsc Advances* 5 (44) (2015) 35138–35154.
- 720 [16] T. T. Reddy, L. Lavenant, J. Lefebvre, D. Renard, Swelling behavior and controlled release of theophylline and sulfamethoxazole drugs in β -lactoglobulin protein gels obtained by phase separation in water/ethanol mixture, *Biomacromolecules* 7 (1) (2006) 323–330.
- 725 [17] A. S. McAlpine, L. Sawyer, β -Lactoglobulin: a protein drug carrier?, *Biochemical Society Transactions* 18 (5) (1990) 879.
- [18] Y. Mireille, I. van Hille, J.-P. Péliissier, P. Guilloteau, R. Toullec, In vivo milk digestion in the calf abomasum. II. Milk and whey proteolysis, *Reproduction Nutrition Développement* 24 (6) (1984) 835–843.
- 730 [19] R. S. H. Lam, M. T. Nickerson, Food proteins: a review on their emulsifying properties using a structure-function approach, *Food Chemistry* 141 (2) (2013) 975–984.
- [20] W. Lohcharoenkal, L. Wang, Y. C. Chen, Y. Rojanasakul, Protein nanoparticles as drug delivery carriers for cancer therapy, *BioMed Research International* 2014 (2014) 180549.

- 735 [21] W. He, Y. Tan, Z. Tian, L. Chen, F. Hu, W. Wu, Food protein-stabilized nanoemulsions as potential delivery systems for poorly water-soluble drugs: preparation, in vitro characterization, and pharmacokinetics in rats, *International Journal of Nanomedicine* 6 (2011) 521.
- [22] M. C. Yang, H.-H. Guan, J.-M. Yang, C.-N. Ko, M.-Y. Liu, Y.-H. Lin, Y.-
740 C. Huang, C.-J. Chen, S. J. T. Mao, Rational design for crystallization of β -lactoglobulin and vitamin D3 complex: Revealing a secondary binding site, *Crystal Growth and Design* 8 (12) (2008) 4268–4276.
- [23] A. L. Margolin, M. A. Navia, Protein crystals as novel catalytic materials, *Angewandte Chemie International Edition* 40 (12) (2001) 2204–2222.
- 745 [24] F. Zhang, G. Zocher, A. Sauter, T. Stehle, F. Schreiber, Novel approach to controlled protein crystallization through ligandation of yttrium cations, *Journal of Applied Crystallography* 44 (4) (2011) 755–762.
- [25] A. Sauter, F. Roosen-Runge, F. Zhang, G. Lotze, A. Feoktystov, R. M. J. Jacobs, F. Schreiber, On the question of two-step nucleation in protein
750 crystallization, *Faraday Discussions* 179 (2015) 41–58.
- [26] A. Sauter, M. Oelker, G. Zocher, F. Zhang, T. Stehle, F. Schreiber, Non-classical pathways of protein crystallization in the presence of multivalent metal ions, *Crystal Growth and Design* 14 (12) (2014) 6357–6366.
- [27] A. Sauter, F. Roosen-Runge, F. Zhang, G. Lotze, R. M. J. Jacobs,
755 F. Schreiber, Real-time observation of nonclassical protein crystallization kinetics, *Journal of the American Chemical Society* 137 (4) (2015) 1485–1491.
- [28] M. Elias, M. Laranjo, A. C. Agulheiro-Santos, M. E. Potes, The role of salt on food and human health, *Salt in the Earth* (2020) 19.
- 760 [29] R. A. Miller, R. C. Hosney, Role of salt in baking, *Cereal Foods World* 53 (1) (2008) 4–6.

- [30] S. Jeyarajah, J. C. Allen, Calcium binding and salt-induced structural changes of native and preheated β -lactoglobulin, *Journal of Agricultural and Food Chemistry* 42 (1) (1994) 80–85.
- 765 [31] M. E. Richert, G. G. Gochev, B. Braunschweig, Specific ion effects of trivalent cations on the structure and charging state of β -lactoglobulin adsorption layers, *Langmuir* 35 (35) (2019) 11299–11307.
- [32] F. Zhang, F. Roosen-Runge, A. Sauter, R. Roth, M. W. A. Skoda, R. M. J. Jacobs, M. Sztucki, F. Schreiber, The role of cluster formation and metastable liquid-liquid phase separation in protein crystallization, 770 *Faraday Discussions* 159 (2012) 313–325.
- [33] J. Verran, Biofouling in food processing: biofilm or biotransfer potential?, *Food and Bioprocess Technology* 80 (4) (2002) 292–298.
- [34] J. L. Nilsson, Fouling of an ultrafiltration membrane by a dissolved whey protein concentrate and some whey proteins, *Journal of Membrane Science* 775 36 (1988) 147–160.
- [35] A. W. Mohammad, C. Y. Ng, Y. P. Lim, G. H. Ng, Ultrafiltration in food processing industry: review on application, membrane fouling, and fouling control, *Food and Bioprocess Technology* 5 (4) (2012) 1143–1156.
- 780 [36] W. Kunz, Specific ion effects in colloidal and biological systems, *Current Opinion in Colloid & Interface Science* 15 (1-2) (2010) 34–39.
- [37] C. Spitzweg, A. E. Heufelder, J. C. Morris, Thyroid iodine transport, *Thyroid* 10 (4) (2000) 321–330.
- [38] K. Berend, L. H. van Hulsteijn, R. O. Gans, Chloride: the queen of electrolytes?, *European Journal of Internal Medicine* 23 (3) (2012) 203–211. 785
- [39] F. Ahad, S. A. Ganie, Iodine, iodine metabolism and iodine deficiency disorders revisited, *Indian Journal of Endocrinology and Metabolism* 14 (1) (2010) 13.

- [40] Y. M. Efimova, A. A. Van Well, U. Hanefeld, B. Wierczinski, W. G. Bouwman, On the neutron scattering length density of proteins in $\text{H}_2\text{O}/\text{D}_2\text{O}$, *Physica B: Condensed Matter* 350 (1-3) (2004) E877–E880.
- [41] A. Otsuki, L. De Campo, C. J. Garvey, C. Rehm, $\text{H}_2\text{O}/\text{D}_2\text{O}$ contrast variation for ultra-small-angle neutron scattering to minimize multiple scattering effects of colloidal particle suspensions, *Colloids and Interfaces* 2 (3) (2018) 37.
- [42] E. A. Raymond, T. L. Tarbuck, M. G. Brown, G. L. Richmond, Hydrogen-bonding interactions at the vapor/water interface investigated by vibrational sum-frequency spectroscopy of $\text{HOD}/\text{H}_2\text{O}/\text{D}_2\text{O}$ mixtures and molecular dynamics simulations, *The Journal of Physical Chemistry B* 107 (2) (2003) 546–556.
- [43] T. Sato, M. Hashizume, Y. Hotta, Y. Okahata, Morphology and proliferation of B16 melanoma cells in the presence of lanthanoid and Al^{3+} ions, *Biometals* 11 (2) (1998) 107–112.
- [44] J. Y. Lettvin, W. F. Pickard, W. S. McCulloch, W. Pitts, A theory of passive ion flux through axon membranes, *Nature* 202 (4939) (1964) 1338–1339.
- [45] C. R. Triggle, D. J. Triggle, An analysis of the action of cations of the lanthanide series on the mechanical responses of guinea-pig ileal longitudinal muscle, *The Journal of Physiology* 254 (1) (1976) 39–54.
- [46] C. Aussel, R. Marhaba, C. Pelassy, J.-P. Breitmayer, Submicromolar La^{3+} concentrations block the calcium release-activated channel, and impair CD69 and CD25 expression in CD3-or thapsigargin-activated Jurkat cells, *Biochemical Journal* 313 (3) (1996) 909–913.
- [47] A. Zarros, A.-M. Byrne, S. D. Boomkamp, S. Tsakiris, G. S. Baillie, Lanthanum-induced neurotoxicity: solving the riddle of its involvement in cognitive impairment?, *Archives of Toxicology* 87 (11) (2013) 2031–2035.

- [48] M. R. Fries, N. Conzelmann, L. Günter, O. Matsarskaia, M. W. A. Skoda, R. M. J. Jacobs, F. Zhang, F. Schreiber, Bulk phase behaviour vs. interface adsorption: I. specific multivalent cation and anion effects on bsa interactions, *Langmuir* 37 (1) (2021) 139–150.
- [49] F. Zhang, M. W. A. Skoda, R. M. J. Jacobs, S. Zorn, R. A. Martin, C. M. Martin, G. F. Clark, S. Weggler, A. Hildebrandt, O. Kohlbacher, F. Schreiber, Reentrant condensation of proteins in solution induced by multivalent counterions, *Physical Review Letters* 101 (14) (2008) 148101.
- [50] F. Li, J. H.-C. Wang, Q.-M. Wang, Thickness shear mode acoustic wave sensors for characterizing the viscoelastic properties of cell monolayer, *Sensors and Actuators B: Chemical* 128 (2) (2008) 399–406.
- [51] M. Rodahl, B. Kasemo, A simple setup to simultaneously measure the resonant frequency and the absolute dissipation factor of a quartz crystal microbalance, *Review of Scientific Instruments* 67 (9) (1996) 3238–3241.
- [52] C. Steinem, A. Janshoff, *Piezoelectric sensors*, Vol. 5, Springer Science & Business Media, 2007.
- [53] I. Reviakine, D. Johannsmann, R. P. Richter, Hearing what you cannot see and visualizing what you hear: interpreting quartz crystal microbalance data from solvated interfaces, *Analytical Chemistry* 83 (23) (2011) 8838–8848.
- [54] M. V. Voinova, M. Rodahl, M. Jonson, B. Kasemo, Viscoelastic acoustic response of layered polymer films at fluid-solid interfaces: continuum mechanics approach, *Physica Scripta* 59 (5) (1999) 391.
- [55] E. Rojas, M. Gallego, I. Reviakine, Effect of sample heterogeneity on the interpretation of quartz crystal microbalance data: impurity effects, *Analytical Chemistry* 80 (23) (2008) 8982–8990.
- [56] D. Johannsmann, *The quartz crystal microbalance in soft matter research*, Springer, 2015.

- 845 [57] A. Bouhekk, T. Bürgi, In situ ATR-IR spectroscopy study of adsorbed protein: Visible light denaturation of bovine serum albumin on TiO₂, Applied Surface Science 261 (2012) 369–374.
- [58] J. Kong, S. Yu, Fourier transform infrared spectroscopic analysis of protein secondary structures, Acta biochimica et biophysica Sinica 39 (8) (2007) 549–559.
- 850 [59] B. C. Smith, Fundamentals of Fourier transform infrared spectroscopy, CRC press, 2011.
- [60] K. K. Chittur, FTIR/ATR for protein adsorption to biomaterial surfaces, Biomaterials 19 (4-5) (1998) 357–369.
- 855 [61] A. Hughes, GitHub (2019). [link].
URL https://github.com/arwelHughes/RasCAL_2019
- [62] M. Born, E. Wolf, Principles of Optics: Electromagnetic Theory of Propagation, Interference and Diffraction of Light, 6th Edition, Pergamon Press, 1980.
- 860 [63] L. Névot, P. Croce, Caractérisation des surfaces par réflexion rasante de rayons x. application à l’étude du polissage de quelques verres silicates, Revue de Physique Appliquée 15 (3) (1980) 761–779.
- [64] D. S. Sivia, W. A. Hamilton, G. S. Smith, Analysis of neutron reflectivity data: maximum entropy, bayesian spectral analysis and speckle holography, Physica B: Condensed Matter 173 (1-2) (1991) 121–138.
- 865 [65] U. M. Elofsson, M. A. Paulsson, T. Arnebrant, Adsorption of β -Lactoglobulin A and B in relation to self-association: Effect of concentration and pH, Langmuir 13 (6) (1997) 1695–1700.
- [66] O. Matsarskaia, M. K. Braun, F. Roosen-Runge, M. Wolf, F. Zhang, R. Roth, F. Schreiber, Cation-induced hydration effects cause lower critical solution temperature behavior in protein solutions, Journal of Physical Chemistry B 120 (31) (2016) 7731–7736.
- 870

- [67] F. Roosen-Runge, F. Zhang, F. Schreiber, R. Roth, Ion-activated attractive patches as a mechanism for controlled protein interactions, *Scientific Reports* 4 (1) (2014) 7016.
875
- [68] F. Zhang, F. Roosen-Runge, A. Sauter, M. Wolf, R. M. J. Jacobs, F. Schreiber, Reentrant condensation, liquid–liquid phase separation and crystallization in protein solutions induced by multivalent metal ions, *Pure and Applied Chemistry* 86 (2) (2014) 191–202.
- [69] F. Zhang, S. Weggler, M. J. Ziller, L. Ianeselli, B. S. Heck, A. Hildebrandt, O. Kohlbacher, M. W. A. Skoda, R. M. J. Jacobs, F. Schreiber, Universality of protein reentrant condensation in solution induced by multivalent metal ions, *Proteins: Structure, Function, and Bioinformatics* 78 (16) (2010) 3450–3457.
880
- [70] O. Matsarskaia, F. Roosen-Runge, G. Lotze, J. Möller, A. Mariani, F. Zhang, F. Schreiber, Tuning phase transitions of aqueous protein solutions by multivalent cations, *Physical Chemistry Chemical Physics* 20 (42) (2018) 27214–27225.
885
- [71] M. K. Braun, A. Sauter, O. Matsarskaia, M. Wolf, F. Roosen-Runge, M. Sztucki, R. Roth, F. Zhang, F. Schreiber, Reentrant phase behavior in protein solutions induced by multivalent salts: strong effect of anions Cl^- versus NO_3^- , *The Journal of Physical Chemistry B* 122 (50) (2018) 11978–11985.
890
- [72] F. Roosen-Runge, B. S. Heck, F. Zhang, O. Kohlbacher, F. Schreiber, Interplay of pH and binding of multivalent metal ions: charge inversion and reentrant condensation in protein solutions, *The Journal of Physical Chemistry B* 117 (18) (2013) 5777–5787.
895
- [73] M. K. Braun, M. Wolf, O. Matsarskaia, S. Da Vela, F. Roosen-Runge, M. Sztucki, R. Roth, F. Zhang, F. Schreiber, Strong isotope effects on effective interactions and phase behavior in protein solutions in the presence
900

of multivalent ions, *The Journal of Physical Chemistry B* 121 (7) (2017) 1731–1739.

- 905 [74] B. A. Krantz, A. K. Srivastava, S. Nauli, D. Baker, R. T. Sauer, T. R. Sosnick, Understanding protein hydrogen bond formation with kinetic H/D amide isotope effects, *Nature Structural Biology* 9 (6) (2002) 458–463.
- [75] M. Blaber, X. J. Zhang, B. W. Matthews, Structural basis of amino acid alpha helix propensity, *Science* 260 (5114) (1993) 1637–1640.
- [76] Y. M. Efimova, S. Haemers, B. Wierczinski, W. Norde, A. A. van Well, Stability of globular proteins in H₂O and D₂O, *Biopolymers: Original*
910 *Research on Biomolecules* 85 (3) (2007) 264–273.
- [77] P. Cioni, G. B. Strambini, Effect of heavy water on protein flexibility, *Biophysical Journal* 82 (6) (2002) 3246–3253.
- [78] G. C. Kresheck, H. Schneider, H. A. Scheraga, The effect of D₂O on the thermal stability of proteins. Thermodynamic parameters for the transfer
915 of model compounds from H₂O to D₂O, *The Journal of Physical Chemistry* 69 (9) (1965) 3132–3144.
- [79] M. J. Parker, A. R. Clarke, Amide backbone and water-related H/D isotope effects on the dynamics of a protein folding reaction, *Biochemistry* 36 (19) (1997) 5786–5794.
- 920 [80] L. Pérez-Fuentes, C. Drummond, J. Faraudo, D. Bastos-González, Interaction of organic ions with proteins, *Soft Matter* 13 (6) (2017) 1120–1131.
- [81] R. K. Cannan, A. H. Palmer, A. C. Kibrick, The hydrogen ion dissociation curve of β -lactoglobulin, *Journal of Biological Chemistry* 142 (2) (1942) 803–822.
- 925 [82] C. Tanford, Interaction between proteins and chloride ion, *Proceedings of the Iowa Academy of Science* 57 (1) (1950) 225–233.

- [83] I. M. Klotz, J. M. Urquhart, The binding of organic ions by proteins. comparison of native and of modified proteins, *Journal of the American Chemical Society* 71 (5) (1949) 1597–1603.
- 930 [84] L. G. Longsworth, C. F. Jacobsen, An electrophoretic study of the binding of salt ions by β -lactoglobulin and bovine serum albumin., *The Journal of Physical Chemistry* 53 (1) (1949) 126–134.
- [85] E. Brand, Amino acid composition of simple proteins, *Annals of the New York Academy of Sciences* 47 (2) (1946) 187–228.
- 935 [86] C. W. Carr, Studies on the binding of small ions in protein solutions with the use of membrane electrodes. IV. The binding of calcium ions in solutions of various proteins, *Archives of Biochemistry and Biophysics* 46 (2) (1953) 424–431.
- [87] G. B. Jameson, J. J. Adams, L. K. Creamer, Flexibility, functionality
940 and hydrophobicity of bovine β -lactoglobulin, *International Dairy Journal* 12 (4) (2002) 319–329.
- [88] P.-Å. Albertsson, Partition between polymer phases, *Journal of Chromatography A* 159 (1) (1978) 111–122.
- [89] C. Tanford, Hydrophobic free energy, micelle formation and the associ-
945 ation of proteins with amphiphiles, *Journal of Molecular Biology* 67 (1) (1972) 59–74.
- [90] S. H. Behrens, D. G. Grier, The charge of glass and silica surfaces, *The Journal of Chemical Physics* 115 (14) (2001) 6716–6721.
- [91] R. Williams, A. M. Goodman, Wetting of thin layers of SiO_2 by water,
950 *Applied Physics Letters* 25 (10) (1974) 531–532.
- [92] M. Rodahl, P. Dahlqvist, F. Höök, B. Kasemo, The quartz crystal microbalance with dissipation monitoring (QCM-D), in: *Biomolecular Sensors*, Taylor & Francis Inc., 2002, pp. 304–316.

- 955 [93] G. Sauerbrey, Verwendung von Schwingquarzen zur Wägung dünner Schichten und zur Mikrowägung, *Zeitschrift für Physik* 155 (2) (1959) 206–222.
- [94] K. Sakai, Quartz crystal microbalance with dissipation monitoring (QCM-D), in: *Measurement Techniques and Practices of Colloid and Interface Phenomena*, Springer, 2019, pp. 45–50.
- 960 [95] M. R. Fries, D. Stopper, M. K. Braun, A. Hinderhofer, F. Zhang, R. M. J. Jacobs, M. W. A. Skoda, H. Hansen-Goos, R. Roth, F. Schreiber, Multivalent-ion-activated protein adsorption reflecting bulk reentrant behavior, *Physical Review Letters* 119 (22) (2017) 228001.
- 965 [96] M. R. Fries, D. Stopper, M. W. A. Skoda, M. Blum, C. Kertzscher, A. Hinderhofer, F. Zhang, R. M. J. Jacobs, R. Roth, F. Schreiber, Enhanced protein adsorption upon bulk phase separation, *Scientific Reports* 10 (1) (2020) 10349.
- [97] S. X. Liu, J.-T. Kim, Application of Kevin—Voigt model in quantifying whey protein adsorption on polyethersulfone using QCM-D, *JALA: Journal of the Association for Laboratory Automation* 14 (4) (2009) 213–220.
- 970 [98] F. Höök, B. Kasemo, T. Nylander, C. Fant, K. Sott, H. Elwing, Variations in coupled water, viscoelastic properties, and film thickness of a mefp-1 protein film during adsorption and cross-linking: a quartz crystal microbalance with dissipation monitoring, ellipsometry, and surface plasmon resonance study, *Analytical Chemistry* 73 (24) (2001) 5796–5804.
- 975 [99] T. Steiner, The hydrogen bond in the solid state, *Angewandte Chemie International Edition* 41 (1) (2002) 48–76.
- [100] M. K. Braun, M. Grimaldo, F. Roosen-Runge, I. Hoffmann, O. Czakkel, M. Sztucki, F. Zhang, F. Schreiber, T. Seydel, Crowding-controlled cluster size in concentrated aqueous protein solutions: Structure, self- and
- 980

- collective diffusion, *Journal of Physical Chemistry Letters* 8 (12) (2017) 2590–2596.
- [101] H. Susi, D. M. Byler, Fourier deconvolution of the amide I Raman band of proteins as related to conformation, *Applied Spectroscopy* 42 (5) (1988) 819–826.
- 985 [102] S. Ngarize, H. Herman, A. Adams, N. Howell, Comparison of changes in the secondary structure of unheated, heated, and high-pressure-treated β -lactoglobulin and ovalbumin proteins using Fourier transform Raman spectroscopy and self-deconvolution, *Journal of Agricultural and Food Chemistry* 52 (21) (2004) 6470–6477.
- 990 [103] B. Jachimska, S. Świątek, J. Loch, K. Lewiński, T. Luxbacher, Adsorption effectiveness of β -lactoglobulin onto gold surface determined by quartz crystal microbalance, *Bioelectrochemistry* 121 (2018) 95–104.
- [104] G. Yohannes, S. K. Wiedmer, M. Elomaa, M. Jussila, V. Aseyev, M.-L. Riekkola, Thermal aggregation of bovine serum albumin studied by asymmetrical flow field-flow fractionation, *Analytica Chimica Acta* 675 (2) 995 (2010) 191–198.
- [105] S. Brownlow, J. H. M. Cabral, R. Cooper, D. R. Flower, S. J. Yewdall, I. Polikarpov, A. C. T. North, L. Sawyer, Bovine β -lactoglobulin at 1.8 Å resolution—still an enigmatic lipocalin, *Structure* 5 (4) (1997) 481–495.
- 1000 [106] F. Zhang, M. W. A. Skoda, R. M. J. Jacobs, R. A. Martin, C. M. Martin, F. Schreiber, Protein interactions studied by saxs: effect of ionic strength and protein concentration for bsa in aqueous solutions, *The Journal of Physical Chemistry B* 111 (1) (2007) 251–259.
- 1005 [107] H. A. Sober, *Handbook of biochemistry: selected data for molecular biology*, Chemical Rubber Co., 1968.
- [108] T. Maruyama, S. Katoh, M. Nakajima, H. Nabetani, T. P. Abbott, A. Shono, K. Satoh, FT-IR analysis of BSA fouled on ultrafiltration and

- microfiltration membranes, *Journal of Membrane Science* 192 (1-2) (2001) 201–207.
- 1010 [109] L. R. S. Barbosa, M. G. Ortore, F. Spinozzi, P. Mariani, S. Bernstorff, R. Itri, The importance of protein-protein interactions on the pH-induced conformational changes of bovine serum albumin: a small-angle X-ray scattering study, *Biophysical Journal* 98 (1) (2010) 147–157.
- 1015 [110] X. Arias-Moreno, O. Abian, S. Vega, J. Sancho, A. Velazquez-Campoy, Protein-cation interactions: structural and thermodynamic aspects, *Current Protein and Peptide Science* 12 (4) (2011) 325–338.
- [111] R. G. Huber, J. E. Fuchs, S. von Grafenstein, M. Laner, H. G. Wallnoefer, N. Abdelkader, R. T. Kroemer, K. R. Liedl, Entropy from state probabilities: hydration entropy of cations, *The Journal of Physical Chemistry B* 117 (21) (2013) 6466–6472.
- 1020 [112] P. J. Flory, Thermodynamics of high polymer solutions, *The Journal of Chemical Physics* 10 (1) (1942) 51–61.
- [113] Y. Marcus, *Ion properties*, CRC Press, 1997.
- 1025 [114] A. Mahn, M. E. Lienqueo, J. C. Salgado, Methods of calculating protein hydrophobicity and their application in developing correlations to predict hydrophobic interaction chromatography retention, *Journal of Chromatography A* 1216 (10) (2009) 1838–1844.
- [115] M. E. Lienqueo, A. Mahn, J. A. Asenjo, Mathematical correlations for predicting protein retention times in hydrophobic interaction chromatography, *Journal of Chromatography A* 978 (1-2) (2002) 71–79.
- 1030 [116] A. Kato, T. Matsuda, N. Matsudomi, K. Kobayashi, Determination of protein hydrophobicity using sodium dodecyl sulfate binding method, *Journal of Agricultural and Food Chemistry* 32 (2) (1984) 284–288.

- 1035 [117] A. Kato, S. Nakai, Hydrophobicity determined by a fluorescence probe method and its correlation with surface properties of proteins, *Biochimica et Biophysica Acta (BBA)-Protein structure* 624 (1) (1980) 13–20.
- [118] B. H. J. Hofstee, N. F. Otilio, Non-ionic adsorption chromatography of proteins, *Journal of Chromatography A* 159 (1) (1978) 57–69.
- 1040 [119] A. D. Michie, C. A. Orengo, J. M. Thornton, Analysis of domain structural class using an automated class assignment protocol, *Journal of Molecular Biology* 262 (2) (1996) 168–185.
- [120] A. Bujacz, Structures of bovine, equine and leporine serum albumin, *Acta Crystallographica Section D: Biological Crystallography* 68 (10) (2012) 1278–1289.
- 1045 [121] D. Sehnal, A. S. Rose, J. Koča, S. K. Burley, S. Velankar, Mol*: towards a common library and tools for web molecular graphics, *Eurographics Proceedings* 10 (2018) 29–33.
- [122] W. C. Wimley, S. H. White, Experimentally determined hydrophobicity scale for proteins at membrane interfaces, *Nature Structural Biology* 3 (10) 1050 (1996) 842–848.
- [123] C. W. Carr, Studies on the binding of small ions in protein solutions with the use of membrane electrodes. I. The binding of the chloride ion and other inorganic anions in solutions of serum albumin, *Archives of Biochemistry and Biophysics* 40 (2) 1055 (1952) 286–294.
- [124] M. W. Washabaugh, K. D. Collins, The systematic characterization by aqueous column chromatography of solutes which affect protein stability., *Journal of Biological Chemistry* 261 (27) (1986) 12477–12485.
- 1060 [125] R. Maier, G. Zocher, A. Sauter, S. Da Vela, O. Matsarskaia, R. Schweins, M. Sztucki, F. Zhang, T. Stehle, F. Schreiber, Protein crystallization in the presence of a metastable liquid-liquid phase separation, *Crystal Growth and Design* 20 (12) (2020) 7951–7962.

- 1065 [126] Y. Nozaki, J. A. Reynolds, C. Tanford, The interaction of a cationic detergent with bovine serum albumin and other proteins, *Journal of Biological Chemistry* 249 (14) (1974) 4452–4459.
- [127] M. Yamasaki, H. Yano, K. Aoki, Differential scanning calorimetric studies on bovine serum albumin: II. Effects of neutral salts and urea, *International Journal of Biological Macromolecules* 13 (6) (1991) 322–328.
- 1070 [128] H. I. Okur, J. Hladilkova, K. B. Rembert, Y. Cho, J. Heyda, J. Dzubiella, P. S. Cremer, P. Jungwirth, Beyond the Hofmeister series: Ion-specific effects on proteins and their biological functions, *The Journal of Physical Chemistry B* 121 (9) (2017) 1997–2014.
- 1075 [129] K. D. Collins, Ions from the hofmeister series and osmolytes: effects on proteins in solution and in the crystallization process, *Methods* 34 (3) (2004) 300–311.
- [130] F. Karush, Heterogeneity of the binding sites of bovine serum albumin, *Journal of the American Chemical Society* 72 (6) (1950) 2705–2713.
- 1080 [131] L. Pérez-Fuentes, C. Drummond, J. Faraudo, D. Bastos-González, Adsorption of milk proteins (β -casein and β -lactoglobulin) and BSA onto hydrophobic surfaces, *Materials* 10 (8) (2017) 893.
- [132] B. Jachimska, K. Tokarczyk, M. Łapczyńska, A. Puciul-Malinowska, S. Zapotoczny, Structure of bovine serum albumin adsorbed on silica investigated by quartz crystal microbalance, *Colloids and Surfaces A: Physicochemical and Engineering Aspects* 489 (2016) 163–172.
- 1085 [133] N. Begam, O. Matsarskaia, M. Sztucki, F. Zhang, F. Schreiber, Unification of lower and upper critical solution temperature phase behavior of globular protein solutions in the presence of multivalent cations, *Soft Matter* 16 (8) (2020) 2128–2134.

- 1090 [134] A. C. Dumetz, A. M. Chockla, E. W. Kaler, A. M. Lenhoff, Protein phase behavior in aqueous solutions: crystallization, liquid-liquid phase separation, gels, and aggregates, *Biophysical Journal* 94 (2) (2008) 570–583.